

Fundamental limits on the rate of bacterial cell division

Nathan M. Belliveau^{†, 1}, Griffin Chure^{†, 2, 3}, Christina L. Hueschen⁴, Hernan G. Garcia⁵, Jané Kondev⁶, Daniel S. Fisher⁷, Julie Theriot^{1, 8}, Rob Phillips^{2, 9, *}

*For correspondence:

[†]These authors contributed equally to this work

¹Department of Biology, University of Washington, Seattle, WA, USA; ²Division of Biology and Biological Engineering, California Institute of Technology, Pasadena, CA, USA; ³Department of Applied Physics, California Institute of Technology, Pasadena, CA, USA; ⁴Department of Chemical Engineering, Stanford University, Stanford, CA, USA; ⁵Department of Molecular Cell Biology and Department of Physics, University of California Berkeley, Berkeley, CA, USA; ⁶Department of Physics, Brandeis University, Waltham, MA, USA; ⁷Department of Applied Physics, Stanford University, Stanford, CA, USA; ⁸Allen Institute for Cell Science, Seattle, WA, USA; ⁹Department of Physics, California Institute of Technology, Pasadena, CA, USA; *Contributed equally

14

Abstract This will be written next

16

Uptake of Nutrients

In order to build new cellular mass, the molecular and elemental building blocks must be scavenged from the environment in different forms. Carbon, for example, is acquired via the transport of carbohydrates and sugar alcohols with some carbon sources receiving preferential treatment in their consumption (*Monod, 1947*). Phosphorus, sulfur, and nitrogen, on the other hand, are harvested primarily in the forms of inorganic salts, namely phosphate, sulfate, and ammonia (*Jun et al., 2018; Assentoft et al., 2016; Stasi et al., 2019; Antonenko et al., 1997; Rosenberg et al., 1977; Willsky et al., 1973*). All of these compounds have different permeabilities across the cell membrane and most require some energetic investment either via ATP hydrolysis or through the proton electrochemical gradient to bring the material across the hydrophobic cell membrane. Given the diversity of biological transport mechanisms and the vast number of inputs needed to build a cell, we begin by considering transport of some of the most important cellular ingredients: carbon, nitrogen, oxygen, hydrogen, phosphorus, and sulfur.

The elemental composition of *E. coli* has received much quantitative attention over the past half century (*Neidhardt et al., 1991; Taymaz-Nikerel et al., 2010; Heldal et al., 1985; Bauer and Ziv, 1976*), providing us with a starting point for estimating the copy numbers of various transporters. While there is some variability in the exact elemental percentages (with different uncertainties), we can estimate that the dry mass of a typical *E. coli* cell is $\approx 45\%$ carbon (BNID: 100649, *Milo et al. (2010)*), $\approx 15\%$ nitrogen (BNID: 106666, *Milo et al. (2010)*), $\approx 3\%$ phosphorus (BNID: 100653, *Milo et al. (2010)*), and 1% sulfur (BNID: 100655, *Milo et al. (2010)*). In the coming paragraphs, we will engage in a dialogue between back-of-the-envelope estimates for the numbers of transporters needed to facilitate these chemical stoichiometries and the experimental proteomic measurements of the biological reality. Such an approach provides the opportunity to test if our biological knowledge is sufficient to understand the scale at which these complexes are produced. Specifically, we will make these estimates considering a modest doubling time of 5000 s, a growth rate of $\approx 0.5 \text{ hr}^{-1}$,

42 the range in which the majority of the experimental measurements reside.

43 **Nitrogen Transport**

44 Before we begin our back-of-the-envelope estimations, we must address which elemental sources
 45 must require proteinaceous transport, meaning that the cell cannot acquire appreciable amounts
 46 simply via diffusion from the membrane. The permeability of the lipid membrane to a large
 47 number of solutes has been extensively characterized over the past century. Large, polar molecular
 48 species (such as various sugar molecules, sulfate, and phosphate) have low permeabilities while
 49 small, non-polar compounds (such as oxygen, carbon dioxide, and ammonia) can readily diffuse
 50 across the membrane. Ammonia, a primary source of nitrogen in typical laboratory conditions,
 51 has a permeability on par with water ($\approx 10^5$ nm/s, BNID:110824 *Milo et al. (2010)*). In particularly
 52 nitrogen-poor conditions, *E. coli* expresses a transporter (AmtB) which appears to aid in nitrogen
 53 assimilation, though the mechanism and kinetic details of transport is still a matter of debate (*van*
 54 *Heeswijk et al., 2013; Khademi et al., 2004*). Beyond ammonia, another plentiful source of nitrogen
 55 come in the form of glutamate, which has its own complex metabolism and scavenging pathways.
 56 However, nitrogen is plentiful in the growth conditions examined in this work, permitting us to
 57 neglect nitrogen transport as a potential rate limiting process in cell division in typical experimental
 58 conditions. We direct the reader to the supplemental information for a more in-depth discussion of
 59 permeabilities and a series of calculations revealing that active nitrogen transport can be neglected
 60 for the purposes of this article.

61 **Carbon Transport**

62 We begin our estimations with the most abundant element in *E. coli* by mass, carbon. Using
 63 ≈ 0.3 pg as the typical *E. coli* dry mass (BNID: 103904, *Milo et al. (2010)*), we estimate that \approx
 64 10^{10} carbon atoms must be brought into the cell in order to double all of the carbon-containing
 65 molecules (*Figure 1(A, top)*). Typical laboratory growth conditions, such as those explored in the
 66 aforementioned proteomic data sets, provide carbon as a single class of sugar such as glucose,
 67 galactose, or xylose to name a few. *E. coli* has evolved myriad mechanisms by which these sugars can
 68 be transported across the cell membrane. One such mechanism of transport is via the PTS system
 69 which is a highly modular system capable of transporting a diverse range of sugars (*Escalante*
 70 *et al., 2012*). The glucose-specific component of this system transports ≈ 200 glucose molecules
 71 per second per channel (BNID: 114686, *Milo et al. (2010)*). Making the assumption that this is a
 72 typical sugar transport rate, coupled with the need to transport 10^{10} carbon atoms, we arrive at the
 73 conclusion that on the order of 1,000 transporters must be expressed in order to bring in enough
 74 carbon atoms to divide in 5000 s, diagrammed in the top panel of *Figure 1(A)*. This estimate, along
 75 with the observed average number of the PTS system carbohydrate transporters present in the
 76 proteomic data sets (*Schmidt et al., 2016; Peebo et al., 2015; Valgepea et al., 2013; Li et al., 2014*),
 77 is shown in *Figure 1(A)*. While we estimate 1500 transporters are needed with a 5000 s division
 78 time, we can abstract this calculation to consider any particular growth rate given knowledge of
 79 the cell density and volume as a function of growth rate and direct the reader to the SI for more
 80 information. As revealed in *Figure 1(A)*, experimental measurements exceed the estimate by several
 81 fold, illustrating that transport of carbon in to the cell is not rate limiting for cell division.

82 The estimate presented in *Figure 1(A)* neglects any specifics of the regulation of carbon transport
 83 system and presents a data-averaged view of how many carbohydrate transporters are present
 84 on average. Using the diverse array of growth conditions explored in the proteomic data sets, we
 85 can explore how individual carbon transport systems depend on the population growth rate. In
 86 *Figure 1(B)*, we show the total number of carbohydrate transporters specific to different carbon
 87 sources. A striking observation, shown in the top-left plot of *Figure 1(B)*, is the constancy in the
 88 expression of the glucose-specific transport systems. Additionally, we note that the total number
 89 of glucose-specific transporters is tightly distributed $\approx 10^4$ per cell, the approximate number of
 90 transporters needed to sustain rapid growth of several divisions per hour, as indicated by the grey

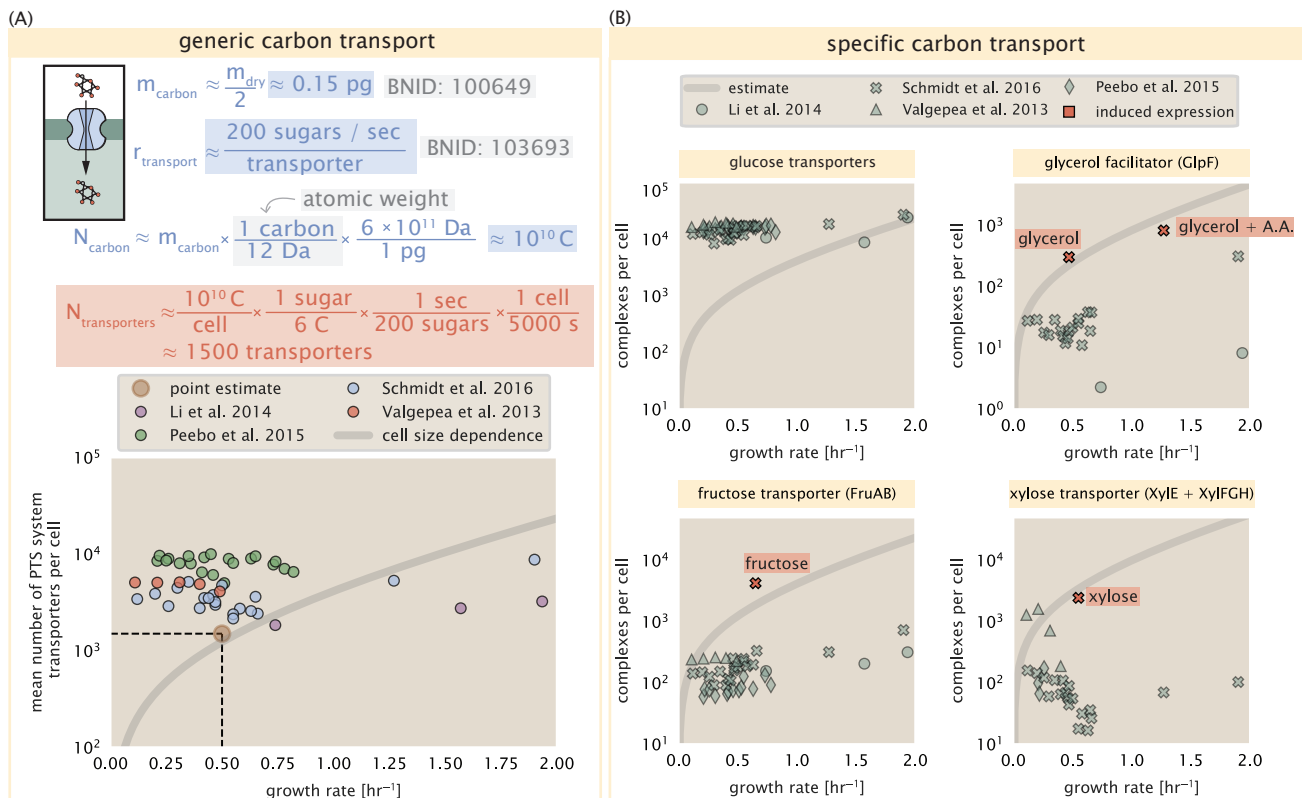


Figure 1. The abundance of carbon transport systems across growth rates. (A) A simple estimate for the minimum number of generic carbohydrate transport systems (top) assumes $\approx 10^{10}$ C are needed to complete division, each transported sugar contains ≈ 6 C, and each transporter conducts sugar molecules at a rate of ≈ 200 per second. Bottom plot shows the estimated number of transporters needed at a growth rate of ≈ 0.5 per hr (light-brown point and dashed lines). Colored points correspond to the mean number of PTS system sugar transporters (complexes annotated with the Gene Ontology term GO:0009401) for different growth conditions across different published datasets. (B) The abundance of various specific carbon transport systems plotted as a function of the population growth rate. Red points and red-highlighted text indicate conditions in which the only source of carbon in the growth medium induces expression of the transport system. Grey line in (A) and (B) represents the estimated number of transporters per cell at a continuum of growth rates.

shaded line. This illustrates that *E. coli* maintains a substantial number of complexes present for transporting glucose which is known to be the preferential carbon source (*Monod, 1947; Liu et al., 2005; Aidelberg et al., 2014*).

It is now understood that a large number of metabolic operons are regulated with dual-input logic gates that are only expressed when glucose concentrations are low (mediated by cyclic-AMP receptor protein CRP) and the concentration of other carbon sources are elevated (*Gama-Castro et al., 2016; Zhang et al., 2014b*). A famed example of such dual-input regulatory logic is in the regulation of the *lac* operon which is only natively activated in the absence of glucose and the presence of allolactose, an intermediate in lactose metabolism (*Jacob and Monod, 1961*), though we now know of many other such examples (*Ireland et al., 2020; Gama-Castro et al., 2016; Belliveau et al., 2018*). This illustrates that once glucose is depleted from the environment, cells have a means to dramatically increase the abundance of the specific transporter needed to digest the next sugar that is present. Several examples of induced expression of specific carbon-source transporters are shown in *Figure 1(B)*. Points colored in red (labeled by red text-boxes) correspond to growth conditions in which the specific carbon source (glycerol, xylose, or fructose) is present. These plots show that, in the absence of the particular carbon source, expression of the transporters is maintained on the order of $\sim 10^2$ per cell. However, when induced, the transporters become highly-expressed and fall close to the predicted number of transporters needed to facilitate growth on that substrate alone, shown as a transparent grey line. Together, this generic estimation and the specific examples of induced expression suggest that transport of carbon across the cell membrane, while critical for growth, is not the rate-limiting step of cell division.

112 Phosphorus and Sulfur Transport

We now turn our attention towards other essential elements, namely phosphorus and sulfur. Phosphorus is critical to the cellular energy economy in the form of high-energy phosphodiester bonds making up DNA, RNA, and the NTP energy pool as well as playing a critical role in the post-translational modification of proteins and defining the polar-heads of lipids. In total, phosphorus makes up $\approx 3\%$ of the cellular dry mass which in typical experimental conditions is in the form of inorganic phosphate. The cell membrane has remarkably low permeability to this highly-charged and critical molecule, therefore requiring the expression of active transport systems. In *E. coli*, the proton electrochemical gradient across the inner membrane is leveraged to transport inorganic phosphate into the cell (*Rosenberg et al., 1977*). Proton-solute symporters are widespread in *E. coli* (*Ramos and Kaback, 1977; Booth et al., 1979*) and can have rapid transport rates of 50 to 100 molecules per second for sugars and other solutes (BNID: 103159; 111777, *Milo et al. (2010)*). As a more extreme example, the proton transporters in the F₁-F₀ ATP synthase, which leverage the proton electrochemical gradient for rotational motion, can shuttle protons across the membrane at a rate of ≈ 1000 per second (BNID: 104890; 103390, *(Milo et al., 2010)*). In *E. coli* the PitA phosphate transport system has been shown to very tightly coupled with the proton electrochemical gradient with a 1:1 proton:phosphate stoichiometric ratio (*Harris et al., 2001; Feist et al., 2007*). Taking the geometric mean of the aforementioned estimates gives a plausible rate of phosphate transport on the order of 300 per second. Illustrated in *Figure 2(A)*, we can estimate that ≈ 150 phosphate transporters are necessary to maintain an $\approx 3\%$ dry mass with a 5000 s division time. This estimate is again satisfied when we examine the observed copy numbers of PitA in proteomic data sets (plot in *Figure 2(A)*). While our estimate is very much in line with the observed numbers, we emphasize that this is likely a slight over estimate of the number of transporters needed as there are other phosphorous scavenging systems, such as the ATP-dependent phosphate transporter Pst system which we have neglected.

Satisfied that there are a sufficient number of phosphate transporters present in the cell, we now turn to sulfur transport as another potentially rate limiting process. Similar to phosphate, sulfate is highly-charged and not particularly membrane permeable, requiring active transport. While there exists a H⁺/sulfate symporter in *E. coli*, it is in relatively low abundance and is not well

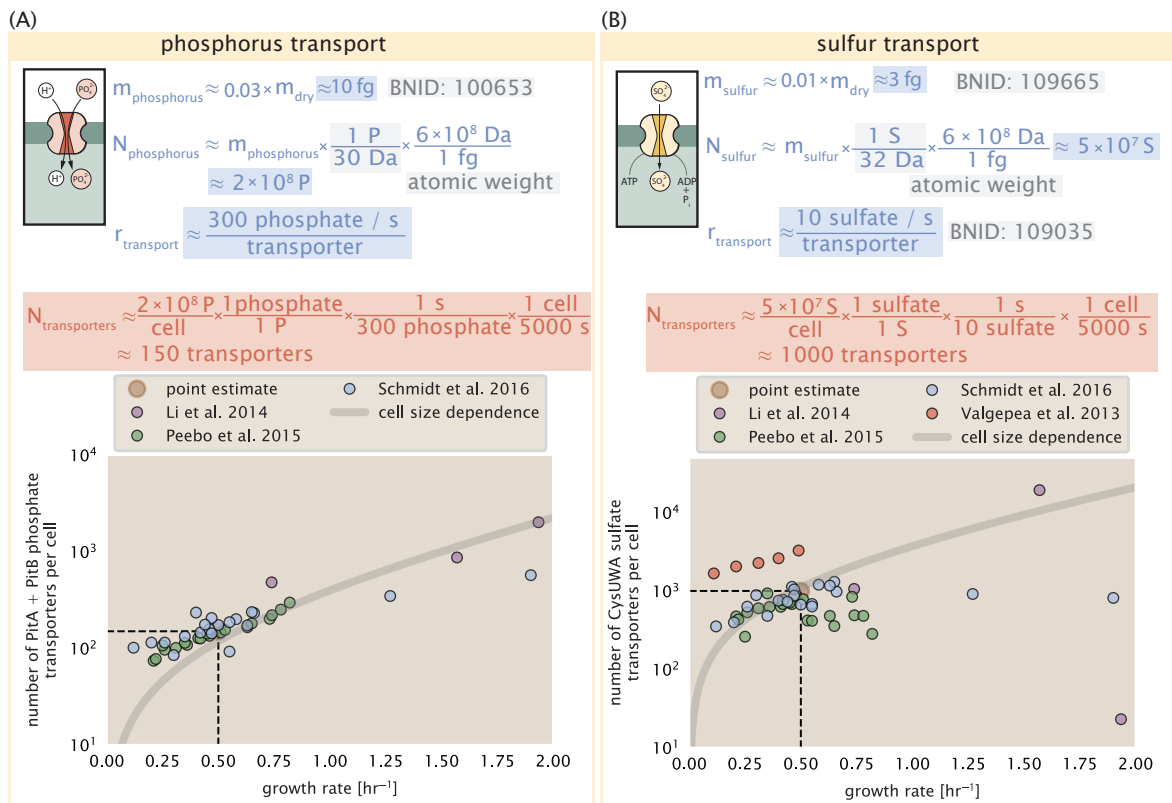


Figure 2. Estimates and measurements of phosphate and sulfate transport systems as a function of growth rate. (A) Estimate for the number of PitA phosphate transport systems needed to maintain a 3% phosphorus *E. coli* dry mass. Points in plot correspond to the total number of PitA transporters per cell. (B) Estimate of the number of CysUWA complexes necessary to maintain a 1% sulfur *E. coli* dry mass. Points in plot correspond to average number of CysUWA transporter complexes that can be formed given the transporter stoichiometry [CysA]₂[CysU][CysW][Sbp/CysP]. Grey line in (A) and (B) represents the estimated number of transporters per cell at a continuum of growth rates.

characterized (Zhang et al., 2014a). Sulfate is predominantly acquired via the ATP-dependent ABC transporter CysUWA system which also plays an important role in selenium transport (Sekowska et al., 2000; Sirko et al., 1995). While specific kinetic details of this transport system are not readily available, generic ATP transport systems in prokaryotes transport on the order of 1 to 10 molecules per second (BNID: 109035, Milo et al. (2010)). Combining this generic transport rate, measurement of sulfur comprising 1% of dry mass, and a 5000 second division time yields an estimate of ≈ 1000 CysUWA complexes per cell (Figure 2(B)). Once again, this estimate is in notable agreement with proteomic data sets, suggesting that there are sufficient transporters present to acquire the necessary sulfur. In a similar spirit of our estimate of phosphorus transport, we emphasize that this is likely an overestimate of the number of necessary transporters as we have neglected other sulfur scavenging systems that are in lower abundance.

152 Limits on Transporter Expression

So which, if any, of these processes may be rate limiting for growth? As suggested by ?? (B), induced expression can lead to an order-of-magnitude (or more) increase in the amount of transporters needed to facilitate transport. Thus, if acquisition of nutrients was the limiting state in cell division, could expression simply be increased to accommodate faster growth? A way to approach this question is to compute the amount of space in the bacterial membrane that could be occupied by nutrient transporters. Considering a rule-of-thumb for the surface area of *E. coli* of about 6 μm^2 (BNID: 101792, Milo et al. (2010)), we expect an areal density for 1000 transporters to be approximately 200 transporters/ μm^2 . For a typical transporter occupying about 50 nm²/dimer, this

amounts to about only 1 percent of the total inner membrane (*Szenk et al., 2017*). In addition, bacterial cell membranes typically have densities of 10^5 proteins/ μm^2 (*Phillips, 2018*), implying that the cell could accommodate more transporters of a variety of species if it were rate limiting. As we will see in the next section, however, occupancy of the membrane can impose other limits on the rate of energy production.

166 Protein synthesis

167 Lastly, we turn our attention to the process of translation. So far our estimates have led to protein
 168 copy numbers that are consistent with the proteomic data, or even in excess of what might be
 169 needed for each task under limiting growth conditions. Even in our example of *E. coli* grown under
 170 different carbohydrate sources (*Figure 1(B)*), cells can utilize alternative carbon sources by inducing
 171 the expression of additional membrane transporters and enzymes. Optimal resource allocation
 172 and the role of ribosomal proteins have been an area of intense quantitative study over the last
 173 decade by Hwa and others (*Scott et al., 2010; Hui et al., 2015*). From the perspective of limiting
 174 growth, our earlier estimate of rRNA highlighted the necessity for multiple copies of rRNA genes in
 175 order to make enough rRNA, suggesting the possibility that synthesis of ribosomes might be rate
 176 limiting. While the transcriptional demand for the ribosomal proteins is substantially lower than
 177 rRNA genes, since proteins can be translated from relatively fewer mRNA, other ribosomal proteins
 178 like the translation elongation factor EF-Tu also present a substantial burden. For EF-Tu in particular,
 179 it is the most highly expressed protein in *E. coli* and is expressed from multiple gene copies, tufA
 180 and tufB.

181 We can begin to gain some intuition into how translation might limit growth by noting that the
 182 total number of peptide bonds generated as the cell doubles, N_{aa} , will be given by, $\tau \cdot r_t \cdot R / \ln(2)$.
 183 Here, τ refers to the doubling time of the cell under steady-state growth. The factor $\ln(2)$ is due
 184 to exponential growth of protein mass, with the growth rate $\lambda = \ln(2)/\tau$. r_t is the maximum
 185 translation elongation rate, and R is the average number of ribosomes per cell. We can write the
 186 translation-limited growth rate as,

$$\lambda_{\text{translation-limited}} = \frac{r_t \cdot R}{N_{aa}}. \quad (1)$$

187 Alternatively, since N_{aa} is related to the total protein mass through the molecular weight of each
 188 protein, we can also consider the growth rate in terms of ribosomal mass fraction. By making the
 189 approximation that an average amino acid has a molecular weight of 110 Da (see *Figure 3(A)*), we
 190 can rewrite the growth rate as,

$$\lambda_{\text{translation-limited}} \approx \frac{r_t}{L_R} \Phi_R, \quad (2)$$

191 where L_R is the total length in amino acids that make up a ribosome, and Φ_R is the ribosomal
 192 mass fraction. This is plotted as a function of ribosomal fraction Φ_R in *Figure 3(A)*, where we take
 193 $L_R \approx 7459$ aa, corresponding to the length in amino acids for all ribosomal subunits of the 50S
 194 and 30S complex (BNID: 101175, (*Milo et al., 2010*)). This formulation assumes that the cell can
 195 transcribe the required amount of rRNA, which appears reasonable for *E. coli* under the allowing us
 196 to consider the inherent limit on growth set by the ribosome.

197 The growth rate defined by Equation 2 reflects mass-balance under steady-state growth and
 198 has long provided a rationalization to the apparent linear increase in *E. coli*'s ribosomal content
 199 as a function of growth rate (*Maaløe, 1979; Scott et al., 2010*). For our purposes, there are several
 200 important consequences of this trend. Perhaps the first thing to notice is that there is a maximum
 201 growth rate at about $\lambda \approx 6\text{hr}^{-1}$, or doubling time of about 7 minutes (dashed line). This growth rate
 202 can be viewed as an inherent maximum growth rate due to the need for the cell to double the cell's
 203 entire ribosomal mass. Interestingly, this limit is independent of the absolute number of ribosomes,
 204 but rather is simply given by time to translate an entire ribosome, L_R/r_t . As shown in *Figure 3(B)*, we

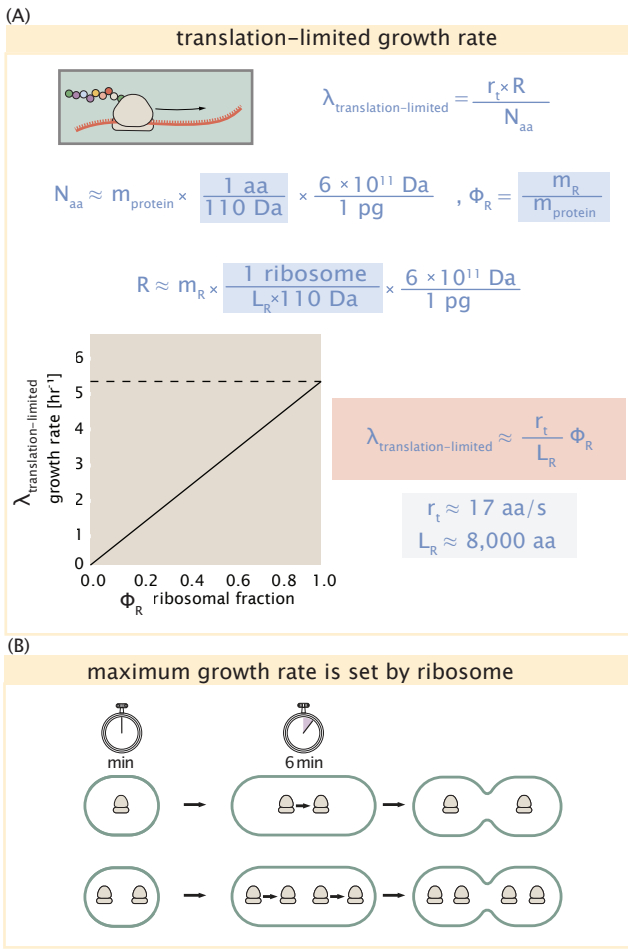


Figure 3. Translation-limited growth rate. (A) Here we consider the translation-limited growth as a function of ribosomal fraction. By mass balance, the time required to double the entire proteome (N_{aa} / r_t) sets the translation-limited growth rate, $\lambda_{\text{translation-limited}}$. Here N_{aa} is effectively the number of peptide bonds that must be translated, r_t is the translation elongation rate, and R is the number of ribosomes. This can also be re-written in terms of the ribosomal mass fraction $\Phi_R = m_R / m_{\text{protein}}$, where m_R is the total ribosomal mass and m_{protein} is the mass of all proteins in the cell. L_R refers to the summed length of the ribosome in amino acids. $\lambda_{\text{translation-limited}}$ is plotted as a function of Φ_R (solid line). (B) The dashed line in part (A) identifies a maximum growth rate that is set by the ribosome. Specifically, this growth rate corresponds to the time required to translate an entire ribosome, L_R / r_t . This is a result that is independent of the number of ribosomes in the cell as shown schematically here.

205 can reconcile this with the observation that in order to double the average number of ribosomes,
206 each ribosome must produce a second ribosome. This is a process that cannot be parallelized.

207 For reasonable values of Φ_R , between about 0.1 - 0.3 (Scott et al., 2010), the maximum growth
208 rate is in line with experimentally reported growth rates around 0.5 - 2 hr⁻¹. Here we are implicitly
209 assuming that translation proceeds randomly, without preference between ribosomal or non-
210 ribosomal mRNA, which appears reasonable. Importantly, in order for a cell to scale this growth
211 limit set by Φ_R , cells *must* increase their ribosomal abundance. This can be achieved by either
212 synthesizing more ribosomes or reducing the fraction of non-ribosomal proteins. Reduction of
213 non-ribosomal proteins is not straight forward since, as we have found throughout our estimates,
214 doubling a cell requires many other enzymes and transporters. Increasing the absolute ribosomal
215 abundance for the case of *E. coli* is limited by the number of rRNA operons.

216 **Multiple replication forks help bias ribosome abundance.**

217 *E. coli* cells grow by an adder mechanism, whereby cells add a constant volume with each cell
218 division (Taheri-Araghi et al., 2015). In conjunction with this, additional rounds of DNA replication
219 are triggered when cells reach a critical volume per origin of replication (Figure 4(A)). This leads to

the classically-described exponential increase in cell size with growth rate **Schaechter et al. (1958)**; **Si et al. (2017, 2019)**. The mechanism behind growth rate control however, has remained elusive. In the context of maximizing growth rate, it is notable that the majority of ribosomal proteins and rRNA operons are found closer to the DNA origin. Given that cells must increase their total gene dosage of rRNA operons at faster growth rates, and the intimate relationship between ribosomal content and growth rate considered above, this raises the possibility that the increase in chromosomal content might simply be a means for the cell to tune biosynthesis according to its physiological state and the nutrient availability in its environment.

While an increase in transcription has been observed for genes closer to the origin in rapidly growing *E. coli* (**Scholz et al., 2019**), we were unaware of such characterization at the proteomic level. In order to see whether there is a relative increase in protein expression for genes closer to the origin at faster growth, we calculated a running boxcar average of protein copy number as a function of each gene's transcriptional start site. While absolute protein copy numbers can vary substantially across the chromosome, we indeed observe a bias in expression under fast growth conditions (**Figure 4(B)**, showing the result using a 0.5 Mb averaging window). The dramatic change in protein copy number near the origin mainly reflects the increase in ribosomal protein expression. This trend is in contrast to slower growth conditions where the average copy number is more uniform across the length of the chromosome.

If ribosomal genes (rRNA and ribosomal proteins) are being maximally synthesized according to the rRNA gene dosage we can make two related hypotheses about how their ribosome abundance should vary with chromosomal content. The first is that the ribosomal protein fraction should increase in proportion to the average ratio of DNA origins to DNA termini ($\langle \# \text{ ori} \rangle / \langle \# \text{ ter} \rangle$ ratio). This is a consequence of the skew in DNA dosage as cells grow faster. The second is that the absolute number of ribosomes should increase with the number of DNA origins ($\langle \# \text{ ori} \rangle$), since this will reflect the total gene dosage at a particular growth condition.

In order to test each of these expectations we considered the experimental data from **Si et al. (2017)**, which inferred these parameters for cells under nutrient-limited growth. $\langle \# \text{ ori} \rangle / \langle \# \text{ ter} \rangle$ ratio depends on how quickly chromosomes are replicated relative the cell's doubling time τ and is given by $2^{\tau_C/\tau}$. Here τ_C is the time taken to replicate *E. coli*'s chromosome, referred to as the C period of cell division. In **Figure 4(C)** we plot τ_C versus τ that were measured, with data points in red corresponding to *E. coli* strain MG1655, and blue to strain NCM3722. In their work they also measured the total RNA to protein ratio which reflects ribosomal abundance and we show that data along with other recent measurements from **Dai et al.** Indeed we find that the ribosomal fraction increases with $\langle \# \text{ ori} \rangle / \langle \# \text{ ter} \rangle$ (**Figure 4(C)**). We note a systematic difference in the relative abundances from **Peebo et al.** and **Valgepea et al.** that was inconsistent with a number of other measurements of total RNA-to-protein ratios ($\approx \Phi_R \times 2.1$ **Dai et al. (2016)**) and only show the data from **Schmidt et al.** and **Li et al.** for relative ribosome abundances (see supplemental section XX for a more complete discussion). For the data shown, the ribosomal fraction doesn't increase as much at higher $\langle \# \text{ ori} \rangle / \langle \# \text{ ter} \rangle$. Since several rRNA operons are actually located quite far from the origin, the trend may in part be a consequence of a diminishing increase in rRNA gene dosage at higher $\langle \# \text{ ori} \rangle / \langle \# \text{ ter} \rangle$ ratios.

We can similarly estimate $\langle \# \text{ ori} \rangle$, which depends on how often replication forks are initiated per cell cycle. This is given by the number of overlapping cell cycles, $2^{\tau_{\text{cyc}}/\tau}$, where τ_{cyc} refers to the total time of chromosome replication and cell division. **Figure 4(E)** shows the associated data from **Si et al.**, which we use to estimate $\langle \# \text{ ori} \rangle$ for each growth condition of the proteomic data. In agreement with our expectations, we find that ribosome copy number increases with the estimated $\langle \# \text{ ori} \rangle$ (**Figure 4(F)**).

While it is difficult to distinguish between causality and correlation, the data is at least consistent with the need for cells to increase their effective rRNA gene dosage in order to grow according to the constraint set by Equation 1. These results may also shed some light on the notable increase in ribosomal content that is observed when sublethal doses of antibiotics (**Scott et al., 2010; Dai**

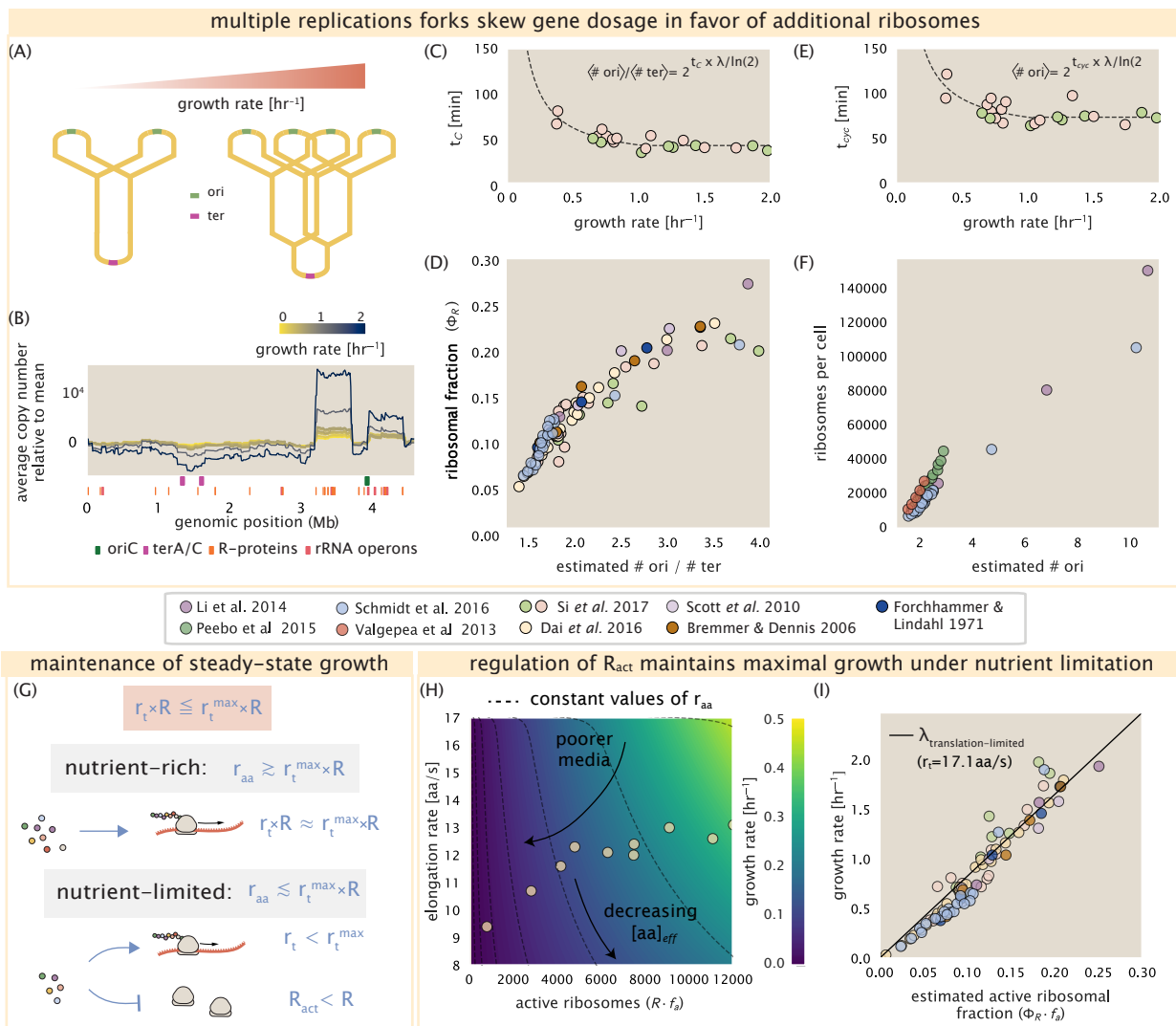


Figure 4. Multiple replication forks skew gene dosage and ribosomal content. (A) Schematic shows the expected increase in replication forks (or number of ori regions) as *E. coli* cells grow faster. (B) A running boxcar average of protein copy number is calculated for each growth condition considered by Schmidt *et al.*. A 0.5 Mb averaging window was used. Protein copy numbers are reported relative to their condition-specific means in order to center all data sets. (C) and (E) show experimental data from Si *et al.* (2017). Solid lines show fits to the data, which were used to estimate $\langle \# \text{ori} \rangle / \langle \# \text{ter} \rangle$ and $\langle \# \text{ori} \rangle$ [NB: to note fit equations]. Red data points correspond to measurements in strain MG1655, while light green points are for strain NCM3722. (D) Plot compares our estimate of $\langle \# \text{ori} \rangle / \langle \# \text{ter} \rangle$ to the experimental measurements of ribosomal abundance. Ribosomal fraction was approximated from the RNA/protein ratios of Dai *et al.* (2016) (yellow) and Si *et al.* (2017) (light red and light green) by the conversion RNA/protein ratio $\approx \Phi_R \cdot 2.1$. (F) Plot of the ribosome copy number estimated from the proteomic data against the estimated $\langle \# \text{ori} \rangle$. (G) Schematic showing translation-specific requirements for maintenance of steady-state growth. In a nutrient rich environment, amino acid supply r_{aa} is sufficiently in excess of demand by ribosomes translating at their maximal rate. In poorer nutrient conditions, reduced amino acid supply r_{aa} will decrease the rate of elongation. In a regime where r_{aa} is less than $r_t \cdot R$, the number of actively translating ribosomes will need to be reduced in order to maintain steady-state growth. (H) Translation elongation rate is plotted as a function of the number of actively translating ribosomes $R \cdot f_a$. Dashed lines correspond to a range of amino acid synthesis rates r_{aa} , from 10^3 to 10^6 . Growth rates are calculated according to Equation 1, assuming a constant ribosomal fraction of 8 percent. See appendix XX for additional details. (I) Experimental data from Dai *et al.* are used to estimate the fraction of actively translating ribosomes. The solid line represents the translation-limited growth rate for ribosomes elongating at 17.1 aa/s.

271 *et al., 2016*). Specifically, if rRNA synthesis is rate limiting, and nutrient conditions largely dictate the
 272 extent of overlapping DNA replication cycles, than addition of antibiotic will lengthen the doubling
 273 time and allow an increase in the abundance of rRNA that can be synthesized relative to the rate of
 274 cell division. In Supplemental Section XX we consider this further using additional data from Si *et al.*
 275 (2017).

276 **Regulation of translating ribosomes helps maintain maximal growth according to
 277 nutrient availability.**

278 While the above analysis provides a possible explanation for how *E. coli* can vary its ribosomal
 279 content to maximize growth, it also presents a challenge in the limit of poorer nutrient conditions.
 280 Recall from Equation 2 that ribosomal content should decrease to zero as growth decreases to zero.
 281 While bacteria tend to decrease their ribosomal abundance in poorer nutrient conditions, they
 282 do so only to some fixed, non-zero amount (*Scott et al., 2010; Lieberman et al., 2014*). Here
 283 we find a minimal ribosomal fraction of about 6 percent in the slowest growth conditions. From
 284 the perspective of a bacterium dealing with uncertain nutrient conditions, there is likely a benefit
 285 for the cell to maintain some relative fraction of ribosomes to support rapid growth as nutrient
 286 conditions improve.

287 The challenge however, lies in the cell's ability to maintain steady-state growth when ribosomes are
 288 in excess of the rate that nutrients can be harvested and amino acids synthesized for consumption
 289 **Figure 4G.** One explanation for this is that the elongation rate decreases in poorer growth conditions.
 290 Cells, however, are still able to maintain a relatively high elongation rate even in stationary phase
 291 ($\approx 8 \text{ aa/s}$, (*Dai et al., 2016, 2018*)). A second explanation is that there are mechanisms to regulate
 292 biological activity in conditions of stress and nutrient-limitation; in particular through the small-
 293 molecule alarmones (p)ppGpp (*Harris and Theriot, 2018*). Here we explore these two observations
 294 to better understand their consequence on growth rate.

295 We consider slow growth conditions (λ less than 0.5 hr^{-1}) by assuming that the decrease in
 296 elongation rate is due to a limiting supply of amino acids and a need for the cell to maintain excess
 297 nutrients for cellular homeostasis under steady-state growth. There is some experimental support
 298 showing that in poorer nutrient growth conditions, cells have lower amino acids concentrations
 299 (*Bennett et al., 2009*). We proceed by coarse grainig the cell's amino acid supply as an single,
 300 effective rate-limiting species (see Appendix XX for a more complete discussion). Under such a
 301 scenario, the elongation rate can described as simply depending on the maximum elongation rate
 302 ($\approx 17.1 \text{ aa/s}$, (*Dai et al., 2016, 2018*)), an effective K_d , and the limiting amino acid concentration
 303 $[aa]_{eff}$. Specifically, the elongation rate is given by,

$$r_t = r_t^{max} \cdot \frac{1}{1 + K_d/[aa]_{eff}}. \quad (3)$$

304 For cells growing in minimal media + glucose, the amino acid concentration is of order 100 mM
 305 (BNID: 110093, (*Milo et al., 2010; Bennett et al., 2009*)). With a growth rate of about 0.6 hr^{-1} and
 306 elongation rate of 12.5 aa per second (*Dai et al., 2016*), we can estimate an effective K_d of about 40
 307 mM. Ultimately the steady state amino acid concentration will depend on the difference between
 308 the supply of amino acids r_{aa} and consumption by ribosomes $r_t \cdot R \cdot f_a$, where f_a accounts for the
 309 possible reduction of actively translating ribosomes.

310 In **Figure 4E** we consider how the maximal growth rate and elongation rates vary as a function of
 311 the number of actively translating ribosomes in this slow growth regime (see Supplemental Section
 312 XX for a complete description of the model). If we consider $r_a a$ to be reflective of a specific growth
 313 condition, by considering lines of constant $r_a a$, we find that cells grow fastest by maximizing their
 314 fraction of actively translating ribosomes. When we consider the experimental measurements from
 315 Dai *et al.*, we see that although cells indeed reduce $R \cdot f_a$, they do so in a way that keeps $[aa]_{eff}$
 316 relatively constant. Given our estimate for the K_d of 40 mM, we would only expect a decrease from
 317 100 mM to about 35 mM in the slowest growth conditions. While experimental data is limited, amino

318 acid concentrations only decrease to about 60 mM for cells grown in minimal media + acetate (λ
 319 0.3 hr^{-1} in our proteomic data; value obtained from **Bennett et al. (2009)**), qualitatively consistent
 320 with our expectations.

321 Given the quantitative data from Dai *et al.*, which determined f_a across the entire range of
 322 growth rates across our data, we next estimated the active fraction of ribosomal protein. As shown
 323 in **Figure 4(G)**, we find that cells grow at a rate near the expected translation maximum expected
 324 from Equation 1, using the maximum elongation rate of $r_t = 17.1 \text{ aa per second}$. This is in contrast
 325 to the reality that ribosomes are translating at almost half this rate in the poorest growth conditions.
 326 This highlights that there are alternative ways to grow according to the translated-limited growth
 327 rate that is expected based with ribosomes translating at their maximal elongation rate. Specifically,
 328 it is by adjusting $r_t \cdot R' \cdot f_a \approx r_{tmax} \cdot R$ that cells are able to scale the growth limit set by Equation 1.

329 [NB, These observations will be very important to include in discussion section: A number of
 330 recent papers highlight the possibility that (p)ppGpp may even provide a causal explanation for
 331 the nutrient-limit scaling law. In the context of ribosomal activity, increased levels of (p)ppGpp are
 332 associated with lower ribosomal content, and at slow growth appear to help reduce the fraction of ac-
 333 tively translating ribosomes (**Dai et al., 2016, 2018**). Titration of the cellular (p)ppGpp concentrations
 334 (up or down) can invoke similar proteomic changes reminiscent of those observed under nutrient
 335 limitation (**Zhu and Dai, 2019**). In light of the limiting dependence of ribosome copy number on
 336 chromosomal gene dosage, it was recently shown that growth in a (p)ppGpp null strain abolishes
 337 both the scaling in cell size and the (# ori) / (# ter) ratio. Instead, cells exhibited a high (# ori) / (#
 338 ter) closer to 4 and cell size more consistent with a fast growth state where (p)ppGpp levels are low
 339 (**Fernández-Coll et al., 2020**).]

340 References

- 341 **Aidelberg G, Towbin BD, Rothschild D, Dekel E, Bren A, Alon U.** Hierarchy of Non-Glucose Sugars in Escherichia
 342 Coli. *BMC Systems Biology*. 2014 Dec; 8(1):133. doi: 10.1186/s12918-014-0133-z.
- 343 **Antonenko YN, Pohl P, Denisov GA.** Permeation of Ammonia across Bilayer Lipid Membranes Studied by
 344 Ammonium Ion Selective Microelectrodes. *Biophysical Journal*. 1997 May; 72(5):2187-2195.
- 345 **Assentoft M, Kaptan S, Schneider HP, Deitmer JW, de Groot BL, MacAulay N.** Aquaporin 4 as a NH3 Channel.
 346 *Journal of Biological Chemistry*. 2016 Sep; 291(36):19184-19195. doi: 10.1074/jbc.M116.740217.
- 347 **Bauer S, Ziv E.** Dense Growth of Aerobic Bacteria in a Bench-Scale Fermentor. *Biotechnology and Bioengineering*. 1976; 18(1):81-94. doi: 10.1002/bit.260180107, _eprint:
 348 https://onlinelibrary.wiley.com/doi/pdf/10.1002/bit.260180107.
- 349 **Belliveau NM, Barnes SL, Ireland WT, Jones DL, Sweredoski MJ, Moradian A, Hess S, Kinney JB, Phillips R.** Systematic Approach for Dissecting the Molecular Mechanisms of Transcriptional Regulation in Bacteria. *Proceedings of the National Academy of Sciences*. 2018 May; 115(21):E4796-E4805. doi: 10.1073/pnas.1722055115.
- 350 **Bennett BD, Kimball EH, Gao M, Osterhout R, Van Dien SJ, Rabinowitz JD.** Absolute metabolite concentrations
 351 and implied enzyme active site occupancy in Escherichia coli. *Nature Chemical Biology*. 2009 Aug; 5(8):593-
 352 599.
- 353 **Booth IR, Mitchell WJ, Hamilton WA.** Quantitative Analysis of Proton-Linked Transport Systems. The Lactose
 354 Permease of Escherichia Coli. *Biochemical Journal*. 1979 Sep; 182(3):687-696.
- 355 **Dai X, Zhu M, Warren M, Balakrishnan R, Okano H, Williamson JR, Fredrick K, Hwa T.** Slowdown of Translational
 356 Elongation in Escherichia coli under Hyperosmotic Stress. - PubMed - NCBI. *mBio*. 2018 Feb; 9(1):281.
- 357 **Dai X, Zhu M, Warren M, Balakrishnan R, Patsalo V, Okano H, Williamson JR, Fredrick K, Wang YP, Hwa T.** Reduction
 358 of translating ribosomes enables Escherichia coli to maintain elongation rates during slow growth. *Nature Microbiology*. 2016 Dec; 2(2):16231.
- 359 **Escalante A, Salinas Cervantes A, Gosset G, Bolívar F.** Current Knowledge of the Escherichia Coli Phosphoenolpyruvate-Carbohydrate Phosphotransferase System: Peculiarities of Regulation and Impact on
 360 Growth and Product Formation. *Applied Microbiology and Biotechnology*. 2012 Jun; 94(6):1483-1494. doi:
 361 10.1007/s00253-012-4101-5.
- 362

- 367 **Feist AM**, Henry CS, Reed JL, Krummenacker M, Joyce AR, Karp PD, Broadbelt LJ, Hatzimanikatis V, Palsson BØ. A
368 Genome-Scale Metabolic Reconstruction for *Escherichia Coli* K-12 MG1655 That Accounts for 1260 ORFs and
369 Thermodynamic Information. *Molecular Systems Biology*. 2007 Jan; 3(1):121. doi: 10.1038/msb4100155.
- 370 **Fernández-Coll L**, Maciąg-Dorszynska M, Tailor K, Vadia S, Levin PA, Szalewska-Palasz A, Cashel M, Dunny GM.
371 The Absence of (p)ppGpp Renders Initiation of *Escherichia coli* Chromosomal DNA Synthesis Independent of
372 Growth Rates. *mBio*. 2020 Apr; 11(2):45.
- 373 **Gama-Castro S**, Salgado H, Santos-Zavaleta A, Ledezma-Tejeida D, Muñiz-Rascado L, García-Sotelo JS, Alquicira-
374 Hernández K, Martínez-Flores I, Pannier L, Castro-Mondragón JA, Medina-Rivera A, Solano-Lira H, Bonavides-
375 Martínez C, Pérez-Rueda E, Alquicira-Hernández S, Porrón-Sotelo L, López-Fuentes A, Hernández-Koutoucheva
376 A, Moral-Chávez VD, Rinaldi F, et al. RegulonDB Version 9.0: High-Level Integration of Gene Regulation,
377 Coexpression, Motif Clustering and Beyond. *Nucleic Acids Research*. 2016 Jan; 44(D1):D133–D143. doi:
378 10.1093/nar/gkv1156.
- 379 **Harris LK**, Theriot JA. Surface Area to Volume Ratio: A Natural Variable for Bacterial Morphogenesis. *Trends in
380 microbiology*. 2018 Oct; 26(10):815–832.
- 381 **Harris RM**, Webb DC, Howitt SM, Cox GB. Characterization of PitA and PitB from *Escherichia coli*. *Journal of
382 Bacteriology*. 2001 Sep; 183(17):5008–5014. doi: 10.1128/JB.183.17.5008-5014.2001.
- 383 **van Heeswijk WC**, Westerhoff HV, Boogerd FC. Nitrogen Assimilation in *Escherichia coli*: Putting Molecular
384 Data into a Systems Perspective. *Microbiology and Molecular Biology Reviews*. 2013 Dec; 77(4):628–695. doi:
385 10.1128/MMBR.00025-13.
- 386 **Heldal M**, Norland S, Tumyr O. X-Ray Microanalytic Method for Measurement of Dry Matter and Elemental
387 Content of Individual Bacteria. *Applied and Environmental Microbiology*. 1985 Nov; 50(5):1251–1257.
- 388 **Hui S**, Silverman JM, Chen SS, Erickson DW, Basan M, Wang J, Hwa T, Williamson JR. Quantitative proteomic
389 analysis reveals a simple strategy of global resource allocation in bacteria. *Molecular Systems Biology*. 2015
390 Feb; 11(2):e784–e784.
- 391 **Ireland WT**, Beeler SM, Flores-Bautista E, Belliveau NM, Sweredoski MJ, Moradian A, Kinney JB, Phillips R.
392 Deciphering the Regulatory Genome of *Escherichia coli*, One Hundred Promoters at a Time. *bioRxiv*. 2020 Jan;
393 doi: 10.1101/2020.01.18.910323.
- 394 **Jacob F**, Monod J. Genetic Regulatory Mechanisms in the Synthesis of Proteins. *Journal of Molecular Biology*.
395 1961 Jun; 3(3):318–356. doi: 10.1016/S0022-2836(61)80072-7.
- 396 **Jun S**, Si F, Pugatch R, Scott M. Fundamental Principles in Bacterial Physiology - History, Recent Progress, and
397 the Future with Focus on Cell Size Control: A Review. *Reports on Progress in Physics*. 2018 May; 81(5):056601.
398 doi: 10.1088/1361-6633/aaa628.
- 399 **Khademi S**, O'Connell J, Remis J, Robles-Colmenares Y, Miercke LJW, Stroud RM. Mechanism of Ammonia
400 Transport by Amt/MEP/Rh: Structure of AmtB at 1.35 Å. *Science*. 2004 Sep; 305(5690):1587–1594. doi:
401 10.1126/science.1101952.
- 402 **Li GW**, Burkhardt D, Gross C, Weissman JS. Quantifying Absolute Protein Synthesis Rates Reveals Principles
403 Underlying Allocation of Cellular Resources. *Cell*. 2014 Apr; 157(3):624–635. doi: 10.1016/j.cell.2014.02.033.
- 404 **Liebermeister W**, Noor E, Flamholz A, Davidi D, Bernhardt J, Milo R. Visual account of protein investment in
405 cellular functions. *Proceedings of the National Academy of Sciences*. 2014 Jun; 111(23):8488–8493.
- 406 **Liu M**, Durfee T, Cabrera JE, Zhao K, Jin DJ, Blattner FR. Global Transcriptional Programs Reveal a Carbon Source
407 Foraging Strategy by *Escherichia Coli*. *Journal of Biological Chemistry*. 2005 Apr; 280(16):15921–15927. doi:
408 10.1074/jbc.M414050200.
- 409 **Maaløe O**. Regulation of the Protein-Synthesizing Machinery—Ribosomes, tRNA, Factors, and So On. Goldberger
410 R, editor, *Gene Expression*; 1979.
- 411 **Milo R**, Jorgensen P, Moran U, Weber G, Springer M. BioNumbers—the Database of Key Numbers in Molecular
412 and Cell Biology. *Nucleic Acids Research*. 2010 Jan; 38(suppl_1):D750–D753. doi: 10.1093/nar/gkp889.
- 413 **Monod J**. The Phenomenon of Enzymatic Adaptation and Its Bearings on Problems of Genetics and Cellular
414 Differentiation. *Growth Symposium*. 1947; 9:223–289.

- 415 **Neidhardt FC**, Ingraham JL, Schaechter M. Physiology of the Bacterial Cell - A Molecular Approach, vol. 1.
416 Elsevier; 1991.
- 417 **Peebo K**, Valgepea K, Maser A, Nahku R, Adamberg K, Vilu R. Proteome Reallocation in *Escherichia coli* with
418 Increasing Specific Growth Rate. *Molecular BioSystems*. 2015; 11(4):1184–1193. doi: 10.1039/C4MB00721B.
- 419 **Phillips R**. Membranes by the Numbers. In: *Physics of Biological Membranes* Cham: Springer, Cham; 2018.p.
420 73–105.
- 421 **Ramos S**, Kaback HR. The Relation between the Electrochemical Proton Gradient and Active Transport in
422 *Escherichia Coli* Membrane Vesicles. *Biochemistry*. 1977 Mar; 16(5):854–859. doi: 10.1021/bi00624a007.
- 423 **Rosenberg H**, Gerdes RG, Chegwidden K. Two Systems for the Uptake of Phosphate in *Escherichia Coli*. *Journal*
424 of *Bacteriology*. 1977 Aug; 131(2):505–511.
- 425 **Schaechter M**, Maaløe O, Kjeldgaard NO. Dependency on Medium and Temperature of Cell Size and Chemical
426 Composition during Balanced Growth of *Salmonella typhimurium*. *Microbiology*. 1958 Dec; 19(3):592–606.
- 427 **Schmidt A**, Kochanowski K, Vedelaar S, Ahrné E, Volkmer B, Callipo L, Knoops K, Bauer M, Aebersold R, Heine-
428 mann M. The Quantitative and Condition-Dependent *Escherichia coli* Proteome. *Nature Biotechnology*. 2016
429 Jan; 34(1):104–110. doi: 10.1038/nbt.3418.
- 430 **Scholz SA**, Diao R, Wolfe MB, Fivenson EM, Lin XN, Freddolino PL. High-Resolution Mapping of the *Escherichia*
431 *coli* Chromosome Reveals Positions of High and Low Transcription. *Cell Systems*. 2019 Mar; 8(3):212–225.e9.
- 432 **Scott M**, Gunderson CW, Mateescu EM, Zhang Z, Hwa T. Interdependence of cell growth and gene expression:
433 origins and consequences. *Science*. 2010 Nov; 330(6007):1099–1102.
- 434 **Sekowska A**, Kung HF, Danchin A. Sulfur Metabolism in *Escherichia Coli* and Related Bacteria: Facts and Fiction.
435 *Journal of Molecular Microbiology and Biotechnology*. 2000; 2(2):34.
- 436 **Si F**, Le Treut G, Sauls JT, Vadia S, Levin PA, Jun S. Mechanistic Origin of Cell-Size Control and Homeostasis in
437 Bacteria. *Current Biology*. 2019 Jun; 29(11):1760–1770.e7. doi: 10.1016/j.cub.2019.04.062.
- 438 **Si F**, Li D, Cox SE, Sauls JT, Azizi O, Sou C, Schwartz AB, Erickstad MJ, Jun Y, Li X, Jun S. Invariance of Initiation Mass
439 and Predictability of Cell Size in *Escherichia coli*. *Current Biology*. 2017 May; 27(9):1278–1287.
- 440 **Sirko A**, Zatyka M, Sadowy E, Hulanicka D. Sulfate and Thiosulfate Transport in *Escherichia Coli* K-12: Evidence
441 for a Functional Overlapping of Sulfate- and Thiosulfate-Binding Proteins. *Journal of Bacteriology*. 1995 Jul;
442 177(14):4134–4136. doi: 10.1128/jb.177.14.4134-4136.1995.
- 443 **Stasi R**, Neves HI, Spira B. Phosphate Uptake by the Phosphonate Transport System PhnCDE. *BMC Microbiology*.
444 2019 Apr; 19. doi: 10.1186/s12866-019-1445-3.
- 445 **Szenk M**, Dill KA, de Graff AMR. Why Do Fast-Growing Bacteria Enter Overflow Metabolism? Testing the
446 Membrane Real Estate Hypothesis. *Cell Systems*. 2017 Aug; 5(2):95–104. doi: 10.1016/j.cels.2017.06.005.
- 447 **Taheri-Araghi S**, Bradde S, Sauls JT, Hill NS, Levin PA, Paulsson J, Vergassola M, Jun S. Cell-size control and
448 homeostasis in bacteria. - PubMed - NCBI. *Current Biology*. 2015 Feb; 25(3):385–391.
- 449 **Taymaz-Nikerel H**, Borujeni AE, Verheijen PJT, Heijnen JJ, van Gulik WM. Genome-Derived Minimal
450 Metabolic Models for *Escherichia Coli* MG1655 with Estimated in Vivo Respiratory ATP Stoichiometry.
451 *Biotechnology and Bioengineering*. 2010; 107(2):369–381. doi: 10.1002/bit.22802, _eprint:
452 https://onlinelibrary.wiley.com/doi/pdf/10.1002/bit.22802.
- 453 **Valgepea K**, Adamberg K, Seiman A, Vilu R. *Escherichia coli* Achieves Faster Growth by Increasing Catalytic and
454 Translation Rates of Proteins. *Molecular BioSystems*. 2013; 9(9):2344. doi: 10.1039/c3mb70119k.
- 455 **Willsky GR**, Bennett RL, Malamy MH. Inorganic Phosphate Transport in *Escherichia Coli*: Involvement of Two
456 Genes Which Play a Role in Alkaline Phosphatase Regulation. *Journal of Bacteriology*. 1973 Feb; 113(2):529–
457 539.
- 458 **Zhang L**, Jiang W, Nan J, Almqvist J, Huang Y. The *Escherichia Coli* CysZ Is a pH Dependent Sulfate Transporter That
459 Can Be Inhibited by Sulfite. *Biochimica et Biophysica Acta (BBA) - Biomembranes*. 2014 Jul; 1838(7):1809–1816.
460 doi: 10.1016/j.bbamem.2014.03.003.

- 461 **Zhang Z**, Aboulwafa M, Saier MH. Regulation of Crp Gene Expression by the Catabolite Repressor/Activator,
462 *Cra*, in *Escherichia coli*. Journal of Molecular Microbiology and Biotechnology. 2014; 24(3):135–141. doi:
463 10.1159/000362722.
- 464 **Zhu M**, Dai X. Growth suppression by altered (p)ppGpp levels results from non-optimal resource allocation in
465 *Escherichia coli*. Nucleic Acids Research. 2019 Mar; 47(9):4684–4693.